Patterns and Interfaces in Dissipative Dynamics

L. M. Pismen
Department of Chemical Engineering and Minerva Center for Nonlinear Physics of Complex Systems, Technion – Israel Institute of Technology, Haifa, Israel

Article Outline

Glossary
Definition of the Subject
Introduction
Stationary Patterns
Moving Interfaces
Wave Patterns
Future Directions
Bibliography

Glossary

Interface An interface separates domains where different stationary states or different patterns prevail. In the latter case, it is also called a domain wall. The interface typically has a finite thickness comparable to a characteristic intrinsic scale of the system but small compared to the overall system size.

Stationary pattern A stationary pattern is formed as a result of an instability to perturbations with a finite wavenumber. It may have any of various spatial structures (striped, square, hexagonal, or quasicrystalline in 2D, lamellar, crystalline or quasicrystalline in 3D) and may slowly evolve in time.

Wave pattern A wave pattern is formed by a combination of waves propagating in one or different directions.

Definition of the Subject

A *pattern* is an inhomogeneous state of a physical system that arises spontaneously under spatially homogeneous conditions. Spontaneous pattern formation has been first observed by Faraday (1831) in vibrated liquid layers and Bénard (1900) in fluids heated from below. Turing (1952) envisaged pattern formation as the mechanism of morphogenesis in living Nature. Some patterns can be described as a collection of patches or domains where one of alternative homogeneous states prevails, separated by relatively narrow *interfaces.* In their turn, moving interfaces may develop corrugation patterns. Patterns can be stationary or wavelike; they can be regular, interlaced by defects, or chaotic (turbulent). In the latter part of twentieth century, numerous pattern formation phenomena have been observed in chemistry, biology, fluid mechanics, granular media, nonlinear optics, and other applications, and common models describing these phenomena in physically dissimilar settings have been formulated and studied. Understanding pattern formation is important both for describing natural self-organization phenomena and for developing manufacturing processes based on self-organization.

Introduction

A typical setup of a non-equilibrium system that may undergo a symmetry-breaking transition is shown in Fig. 1. A non-equilibrium stationary state homogeneous in the "horizontal" plane is sustained by fluxes in the normal ("vertical") direction, along which an inhomogeneous "vertical structure" may be formed. This setup may be realized as a layer of fluid or granular matter; a chemically reacting system, such as an active layer or a catalytic surface; an area where different populations spread out and compete; a propagating interphase boundary, e.g. a

A. Hutt, H. Haken (eds.), *Synergetics*,
https://doi.org/10.1007/978-1-0716-0421-2_381

Originally published in
R. A. Meyers (ed.), *Encyclopedia of Complexity and Systems Science*, © Springer Science+Business Media LLC 2017
https://doi.org/10.1007/978-3-642-27737-5_381-2

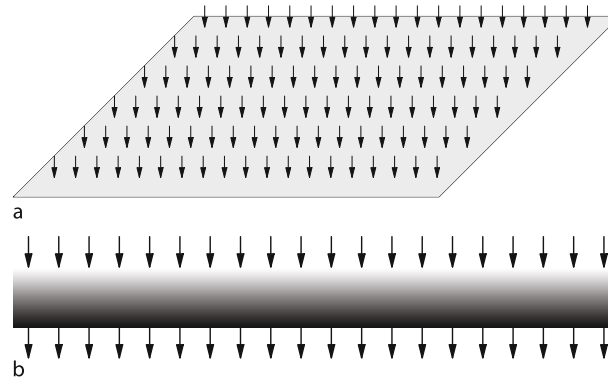

Patterns and Interfaces in Dissipative Dynamics, Fig. 1 An open system isotropic in two dimensions. A truly two-dimensional system (*above*) and a cut through a system with vertical structure (*below,* shown symbolically by *varied shading*). *Arrows* indicate the direction of external fluxes

melting or crystallizing solid; a slice of nonlinear optical medium, etc. Under certain conditions, most commonly, under increased driving, this homogeneous state may be destabilized, giving way to a stationary or moving pattern with a characteristic wavelength dependent on physical properties of the system as well as on external fluxes. In chemically reacting systems, three-dimensional patterns can be also formed when a sufficient amount of reactants is stored; such patterns may exist, of course, for a limited time until the original cache is depleted. Mathematically, a pattern typically emerges as an inhomogeneous solution of a (system of) partial differential equation(s) with space-independent coefficients in the absence of lateral fluxes.

Alternative states, corresponding to different phases, may exist also in equilibrium systems. Following a fast quench past a critical point, different states, separated by domain boundaries, would be approached at spatially removed locations. Typically, these domains would consequently slowly coarsen to minimize the extent of an interphase boundary and related energetic costs. A stationary pattern with a finite wavelength may exist, however, also at equilibrium, provided it minimizes the free energy of the system. Such patterns are realized as "mesoscopic crystals" in block-copolymers consisting of two kinds of mutually repelling units (Hamley 2003).

In fluid mechanics, inhomogeneous states, most often disordered but still retaining a measure of regularity, are commonplace, as anybody observing wavy sea and cloud patterns could have realized long before classical nineteenth century experiments of Faraday and Bénard. Wave patterns generated by oscillatory chemical reactions (which long considered to be impossible due to thermodynamic misconceptions) were demonstrated in 1960s (Burger and Field 1985), while controlled experiments demonstrating persistent stationary chemical patterns in reaction-diffusion systems had to wait till early 1990s (Ouyang and Swinney 1991). Shell growth patterns (Gierer and Meinhard 1972), striped and dotted animal skins (Murray 1981), and desert vegetation patterns (Gilad et al. 2007) have been always here for anybody to observe, before finding rational explanation in terms of the same nonlinear models. Corrugated interfaces were observed and described both as flame fronts in combustion theory (Zeldovich 1985) and as dendrite forms of growing crystals (Langer 1980). More recently, much attention has been drawn by nonlinear optical patterns – spontaneous images emerging in optical circuits and lasers (Arecchi 1999).

Stationary Patterns

Symmetry-Breaking Transitions

The most direct way to formation of stationary patterns is a symmetry-breaking bifurcation. It can be demonstrated in a straightforward way taking as an example a two-component reaction-diffusion system (RDS)

$$\partial_t u = D_1 \nabla^2 u + \gamma_1^{-1} f(u, v), \tag{1}$$

$$\partial_t v = D_2 \nabla^2 v + \gamma_2^{-1} g(u, v), \tag{2}$$

where $f(u, v)$, $g(u, v)$ are source functions depending on the variables u and v, D_1, D_2 are

diffusivities, and ∇^2 is the Laplace operator. We suppose that the system has a homogeneous stationary state (HSS) $u = u_s$, $v = v_s$ satisfying $f(u_s, v_s) = g(u_s, v_s) = 0$; the factors γ_1,γ_2 are introduced to scale the derivatives f_u, g_v computed at this HSS to unity. Stability analysis of the chosen HSS to infinitesimal perturbations $\tilde{u}, \tilde{v} \propto \exp(\mathrm{i}\boldsymbol{k} \cdot \boldsymbol{x})$ with a wave vector $\boldsymbol{k}$ shows that the most dangerous perturbations have the wavenumber

$$|\boldsymbol{k}|^2 \equiv k^2 = \frac{1}{2}\left(\frac{f_u}{\gamma_1 D_1} + \frac{g_v}{\gamma_2 D_2}\right). \quad (3)$$

This value should be positive, which is possible only in the presence of positive feedback, or, in chemical terms, when at least one of the species is "autocatalytic", say, $f_u > 0$ Breaking of spatial symmetry preempts Hopf bifurcation, which occurs at $\gamma_1^{-1} f_u + \gamma_2^{-1} g_v = 0$ and leads to homogeneous oscillations, provided only one of the species is autocatalytic, so that $g_v < 0$, and the autocatalytic species is less diffusive. Thus, for spatial symmetry breaking in a two-component system, one needs a combination of a slowly diffusing "activator" and a rapidly diffusing "inhibitor".

The development of a pattern can be understood qualitatively in the following way. A local upsurge of the activator concentration increases also the concentration of the inhibitor, which spreads out suppressing the activator at neighboring locations. This, in turn, suppresses the inhibitor locally and, through inhibitor diffusion, enhances the activator further along the line, so that the inhomogeneous state spreads out. This scheme works with the roles of an activator and an inhibitor played, respectively, by prey and predator in population dynamics, by growing plants and seeping moisture in ecology, or, rather less directly, by buoyancy and heat conduction in natural convection.

Pattern formation may also result from nonlocal interactions. For example, a nonlocal extension of the nonlinear Schrödinger equation (NLS) for a complex field u,

$$-i\partial_t u = \nabla^2 u - u(\boldsymbol{x}) \int U(\boldsymbol{x} - \boldsymbol{\xi}) |u(\boldsymbol{\xi})|^2 \mathrm{d}\xi, \quad (4)$$

generates a patterned state known as "supersolid", as compared and contrasted to superfluid solutions of the local NLS (Josserand et al. 2007). It might be possible to derive nonlocal equations from a local RDS. Thus, if in Eq. 2 $\gamma_2 << \gamma_1$, so that the inhibitor is fast as well as diffusive, the time derivative can be neglected; then, if the function $g(u, v)$ is linear in v, Eq. 2 can be resolved with the help of an appropriate Green's function, and substituting it in Eq. 1 yields a nonlocal activator equation.

Selection of Stationary Patterns

Symmetry breaking transitions in more than one dimension are degenerate due to spatial symmetries. In an isotropic system, an arbitrary number of differently directed modes with $k = |\boldsymbol{k}| = \text{idem}$ can be excited beyond the bifurcation point. A combination of these modes can give a variety of distinct *planforms*. Competition among the modes that determines the pattern selection is described by *amplitude equations* describing evolution of complex amplitudes a_j, which have a general form

$$\begin{aligned} \frac{\mathrm{d}a_j}{\mathrm{d}t} &= -\frac{\partial V}{\partial \overline{a}_j}, \\ V &= -\mu \sum |a_j|^2 + \sum v_{ijk} a_i a_j a_k \\ &\quad + \sum v_{ijkl} a_i a_j a_k a_l + \text{c.c.} \end{aligned} \quad (5)$$

Here the coefficient μ is proportional to the deviation from the bifurcation point; real coefficients v_{ijk}, v_{ijkl} characterize nonlinear interactions among the modes; the summation is carried out over all closed polygons formed by the wave vectors of extant modes. The product of the amplitudes $\overline{a}_j$, $\overline{a}_k$, etc. (where the overline denotes the complex conjugate) may appear in the equation for the amplitude a_j if the respective wave vectors add up to zero, $\boldsymbol{k}_i + \boldsymbol{k}_j + \boldsymbol{k}_k + \cdots = 0$. This condition ensures that the modes in question are in resonance. Otherwise, the product of these modes rapidly oscillates and is averaged out when the amplitude equation is derived using a multiscale expansion procedure. Stationary solutions, i.e. potential minima of Eq. 5 with one, two, three, or more non-vanishing modes with a symmetric star of wave vectors correspond, respectively, to a striped, square, hexagonal, or quasicrystalline pattern.

The cubic term in the potential (5) generates the lowest-order, hence, strongest nonlinear interactions. This term vanishes in the presence of inversion symmetry $a \rightarrow -a$, which exists, in particular, in the thoroughly studied case of buoyancy-driven convection in the Boussinesq approximation. Otherwise, it is dominant near the bifurcation point, causing (in 2D) a subcritical transition to a hexagonal pattern comprising modes forming a regular triangle. These three modes are in resonance, which means that their phases are not independent but bound by a linear relationship. The sum of phases always adjusts in such a way that interactions are destabilizing. The remaining two phase degrees of freedom correspond to translational symmetry in the plane.

In 3D, the preferred patterns, or crystalline structures, comprise wave vectors forming a regular polyhedron with triangular faces – tetrahedron, octahedron or dodecahedron (Alexander and McTague 1978). The former two correspond to a body- centered cubic (bcc), and the last one, to a quasicrystalline structure with fivefold symmetry. These lowest-order interactions cannot, however, stabilize the pattern at a finite amplitude, and next-order interactions generated by the quartic term in Eq. 5 are necessary to saturate the pattern. Depending on respective interaction coefficients, various structures can be chosen.

A greater variety of patterns may arise if planforms with different wavenumbers k are excited simultaneously. This can be achieved in a most natural way in two-layer systems where the wavelength of the excited pattern depends on the thickness of each layer, as in convection (Proctor and Jones 1988), or different diffusivities, as in a pattern-forming chemical system (Yang et al. 2002). More possibilities arise in nonlinear optics where spatial symmetry breaking may occur on different wavelengths at rather close values of a control parameter (Pampaloni et al. 1997). The resulting coupled amplitude equations can generate a variety of composite planforms, which may have a form of superstructures or quasicrystals. Lowest-order interactions can generate various resonances; no rigid fitting of wavenumbers is required for this, since resonant modes can form an isosceles triangle. Dynamics of mode interactions may be complicated (Pismen and Rubinstein 1999), since the gradient structure of Eq. 5 is, generally, lost.

Regular patterns may suffer various instabilities, which limit the range of admissible wavelengths or lead to a change of the planform through excitation of a non-collinear mode or decay of an extant mode. Wavelength changing instabilities, as a rule, do not saturate and lead to formation of defects.

Modulated and Distorted Patterns

Natural patterns seen both in experiment and simulations are never perfect: their amplitudes may be modulated at distances large compared to the basic wavelength, and they may have various defects: dislocations, disclinations, and domain walls. An example of an imperfect striped pattern is shown in Fig. 2. Variation of local wavelengths is possible because instability spreads out to a finite range of wavenumbers, scaled as the square root of the parametric deviation from the bifurcation point. Other imperfections are a consequence of the rotational symmetry of the system.

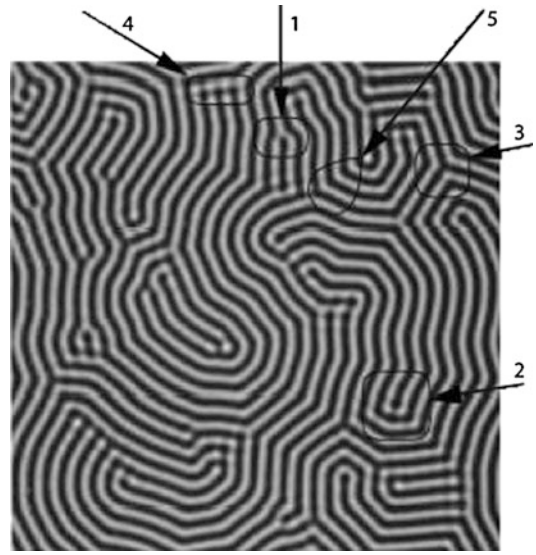

Patterns and Interfaces in Dissipative Dynamics, Fig. 2 Various forms of pattern defects. *1* – dislocation, *2* – concave disclination, *3* – convex disclination, *4* – amplitude domain wall, *5* – phase domain wall (Bowman and Newell 1998, reproduced with permission. Copyright by the American Physical Society)

Different orientations of stripes may be chosen at different locations, either randomly or under influence of boundary conditions or local inhomogeneities. The discrepancies of local orientations are reconciled through formation of disclinations and domain walls, while dislocations reconcile discrepancies of local wavelengths.

Weak distortions, which do not contain defects, can be described by means of either space-dependent amplitude equations applicable to small-amplitude patterns near the bifurcation point, or phase dynamics applicable also to finite-amplitude patterns but restricted to long-scale distortions.

The amplitude equation must have an anisotropic form in an isotropic system, the source of anisotropy being the direction of the wave vector itself. Modulations of this amplitude along and across the direction of the wave vector $\boldsymbol{k}$ should be scaled differently, since adding a small longitudinal component, say, ϵq_x changes $k = |\boldsymbol{k}|$ by $O(\epsilon)$, while adding a transverse component of the same magnitude ϵq_y changes k by $O(\epsilon^2)$ only; thus the stripes are bent far more easily than they are compressed or extended. This leads to the Newell-Whitehead-Segel (NWS) amplitude equation (Newell and Whitehead 1969; Segel 1969), which can be written in a rescaled universal form

$$\partial_t u = \left(\partial_x - \frac{i}{2k}\partial_y^2\right)u + u - |u|^2 u. \qquad (6)$$

The mixed-order differential operator entering this equation precisely accounts for the equivalence of all structures with identical wavenumbers, independently of the direction of the wave vector.

The NWS equation is ill-suited for computations, since the orientation of the coordinate axes depends on the local phase gradient, so that the differential operator is in fact strongly nonlinear. Most model computations of striped patterns are based on the Swift-Hohenberg (SH) equation

$$\partial_t u = -\left(1 + \nabla^2\right)u + u\left(\mu - u^2\right). \qquad (7)$$

In an *anisotropic* system where a certain direction of stripes is preferred, the situation is easier, and the amplitude equation can be reduced by rescaling to an *isotropic* real Ginzburg-Landau (RGL) equation

$$\partial_t u = \nabla^2 u + u - |u|^2 u. \qquad (8)$$

Phase Dynamics

The idea of phase dynamics (Pomeau and Manneville 1979) is to characterize a striped pattern by means of a single variable – phase θ, which changes by 2π over the period of the pattern or, more conveniently, by a rescaled phase $\Theta = \epsilon\theta$. The derivatives of the phase are the wave vector $\boldsymbol{k} = \nabla\theta$ and frequency $\omega = -\theta_t$, which vary on an extended scale exceeding the wavelength of the underlying structure by a factor $\epsilon^{-1} >> 1$. The general form of the phase equation in an isotropic system is determined by scaling and symmetry considerations alone:

$$\partial_T \Theta = D_1\left(\boldsymbol{n}\cdot\hat{\nabla}\right)^2\Theta + D_2\hat{\nabla}^2\Theta, \qquad (9)$$

where $\partial_T, \hat{\nabla}$ are derivatives with respect to slow time and extended spatial variables, $\boldsymbol{n}$ is the unit vector along $\boldsymbol{k}$, and D_1, D_2 are phase diffusivities that depend on a particular underlying problem and are, generally, functions of k. This equation can be also presented in an elegant gradient form (Cross and Newell 1984).

The phase equation (9) is, in fact, strongly nonlinear due to the dependence of both the diffusivities and the direction of the unit vector $\boldsymbol{n}$ on the local phase gradient. It can be linearized, yielding an anisotropic diffusion equation, only when deviations from a prevailing wave vector $\boldsymbol{k} = \boldsymbol{k}_0$ are arbitrary small. If the X- and Y-axes are drawn, respectively, along and across $\boldsymbol{k}_0$, (9) reduces to

$$\Theta_T = D_{||}(k_0)\Theta_{XX} + D_{\perp}(k_0)\Theta_{YY}, \qquad (10)$$

where $D_{||} = D_1 + D_2$ and $D_{\perp} = D_2$ are, respectively, the longitudinal and transverse phase diffusivities. The pattern with the wavenumber k_0 is stable to long-scale perturbations when both phase diffusivities are positive. Vanishing $D_{||}$ corresponds to the *Eckhaus* instability and vanishing $D_{\perp}$ to the *zigzag* instability. Eckhaus instability defines the upper limit of stable wavenumbers. It never

saturates, and usually leads to formation of defects effectively increasing the wavelength. Zigzag instability defines the upper limit of stable wavenumbers; it causes bending of stripes effectively decreasing the wavelength.

Dynamics of Defects

Dynamics of strongly distorted patterns is mostly governed by motion and interaction of defects. Defects are topological objects (Mermin 1979): a dislocation is characterized by circulation of the phase around any enclosing contour equal to an integer multiple of 2π, and a disclination, by circulation of the direction of the wave vector equal to an integer multiple of π. A single dislocation climbing across the direction of the wave vector of a striped pattern effects a change of the wavenumber over an extended region. The force driving the dislocation is due to the deviation from the optimal wavenumber. Eckhaus instability of a striped pattern leads to the formation of a dislocation pair. It is notable that, although the far field of dislocations can be described by phase equations, their interaction is determined by the dislocation core where these equations are inapplicable (Bodenschatz et al. 1988; Pismen and Rodriguez 1990).

Motion of dislocations in striped patterns is well understood and supported by experimental evidence (Braun and Steinberg 1991) for anisotropic patterns governed by Eq. 8. The structure of dislocations in isotropic systems described by Eq. 6 is more complicated, being strongly anisotropic (Nepomnyashchy and Pismen 1991). Disclinations pose more difficulties for the analysis, even on the topological level (Mermin 1979), see (Newell et al. 1996).

Paradoxically, defects enhance relaxation of the pattern to a state of minimum energy corresponding to an "optimal" wavelength. If a deviation of the control parameter from the symmetry breaking bifurcation point is of $O(\epsilon^2)$, the width of the band of excited modes is of $O(\epsilon)$, but the band width actually observed in a natural patterns containing defects is of $O(\epsilon^2)$ (Bowman and Newell 1998). The band shrinks due to motion of point defects and adjustments influenced by domain walls.

The structure and interaction of dislocations in a hexagonal pattern is strongly affected by the resonant character of interactions among the constituent modes. Dislocations in any two modes of the triplet forming a hexagonal pattern, created originally at arbitrary locations, are always attracted to each other (Bodenschatz et al. 2000; Rabinovich and Tsimring 1994), eventually forming an immobile bound pair corresponding to a penta-hepta defect (see Fig. 3).

Equations 6 and 8 are derivable from an energy functional that decreases monotonically in time until a stationary state of minimal energy is reached; this state may still contain defects necessary to satisfy boundary conditions in a confined region. In some cases, however, an additional field, besides the amplitude, is necessary to adequately describe a physical system even close to the symmetry-breaking bifurcation point. A well known example is Bénard convection in low Prandtl number fluids where the additional factor is mean flow generated by pattern distortions and

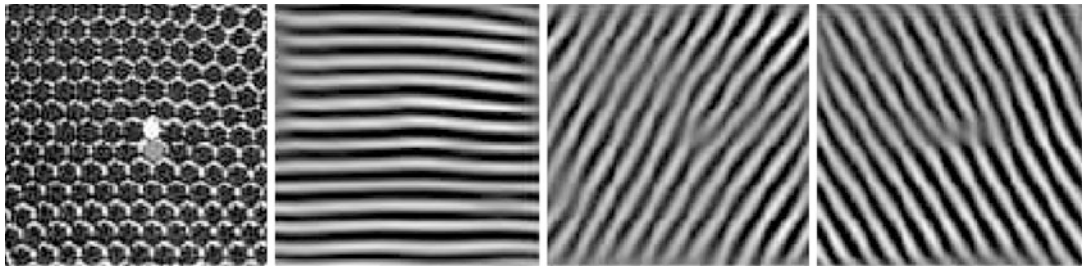

Patterns and Interfaces in Dissipative Dynamics, Fig. 3 Hexagonal pattern containing a penta-hepta defect (*left*) and its three constituent modes obtained by Fourier filtering of the initial image (Abou et al. 2000, reproduced with permission)

advecting the entire pattern. In this case, the patterns remains weakly turbulent indefinitely long, displaying labyrinthine structures, coexisting striped and hexagonal domains (Assenheimer and Steinberg 1993) or spiral defect chaos (Bodenschatz et al. 2000) (see Fig. 4). Chaotic non-stationary patterns also typically appear at higher amplitudes. In reaction-diffusion systems non-stationary and chaotic patterns become more likely when the inhibitor response is slowed down.

Moving Interfaces

Stationary and Propagating Fronts

Many physical systems, either at equilibrium or in a non-equilibrium steady state sustained by external fluxes, may exist in two or more alternative states. If different states are attained at different spatial locations, they are separated by an *interface,* carrying excess energy. The simplest model is a single "reaction-diffusion" equation

$$\partial_t u = D\nabla^2 u + f(u), \tag{11}$$

where D is diffusivity and the function $f(u) = -V'(u)$ (see Fig. 5) has three zeroes that correspond to two stable (with $f'(u) < 0$) and one unstable (with $f'(u) > 0$) HSS. This equation was first used in the context of phase equilibria (van der Waals 1894) as a model of gas-liquid interface, with u denoting density. It was later extended to the solidification problem, with u denoting a fictitious "phase field" assuming its two stable values $u = u_s^{\pm}$ in the liquid and solid phases (Cahn and Hilliard 1958). The coefficient D is interpreted in this context as *rigidity.* The "reaction-diffusion" interpretation applies to non-equilibrium systems, such as a catalytic

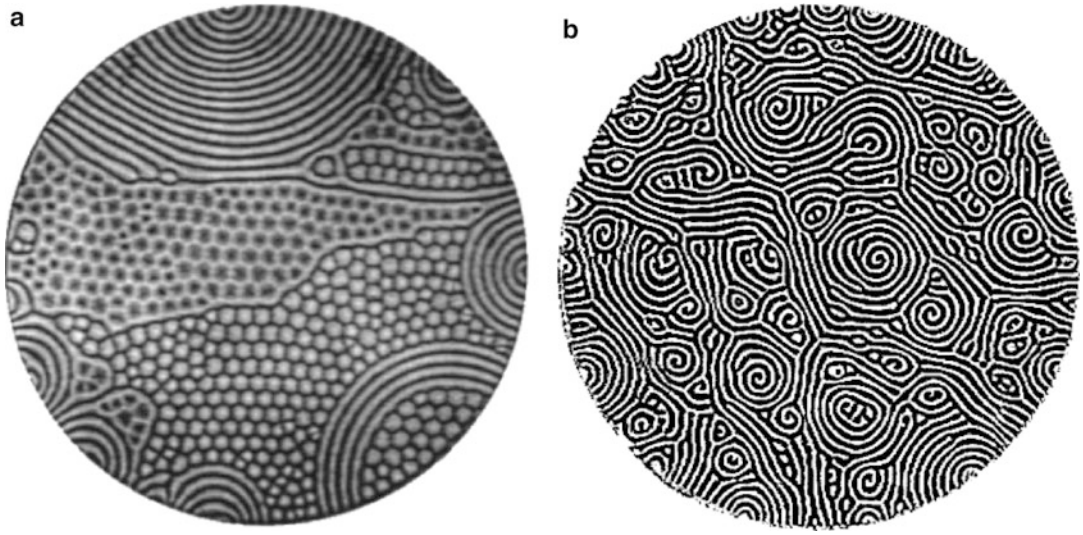

Patterns and Interfaces in Dissipative Dynamics, Fig. 4 (**a**) Coexisting domains; (**b**) Spiral defect chaos (Bodenschatz et al. 2000, reproduced with permission)

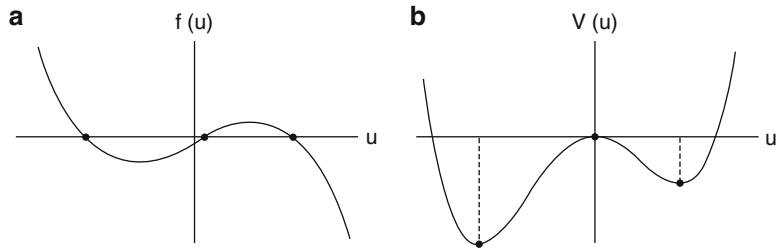

Patterns and Interfaces in Dissipative Dynamics, Fig. 5 A function $f(u)$ with three zeros (**a**) and the respective double-well potential (**b**)

surface or an ecological domain, with u denoting concentration and $f(u)$, the net production rate.
A straight-line or planar interface is stationary when the potentials $V\left(u_s^{\pm}\right)$ are equal. It carries then the interfacial energy

$$\sigma = D\int_{-\infty}^{\infty} u'(x)^2 \mathrm{d}x = \int_{u_s}^{u_s^+} -\sqrt{2DV(u)}\mathrm{d}u, \qquad (12)$$

which is identified with surface tension.

If the potentials are unequal, the front moves in the direction decreasing the total energy of the system. Assuming that the motion is stationary and directed along the x axis, (11) can be rewritten in the comoving frame propagating with the front velocity c. The steadily propagating solution depends on a single coordinate $\xi = x - ct$, and (11) reduces to an ordinary differential equation

$$cu'(\xi) + Du''(\xi) + f(u) = 0, \qquad (13)$$

subject to the boundary conditions $u = u_s^{\pm}$ at $\xi \to \pm\infty$.When both equilibria are stable, they are saddles when viewed as equilibria of (13). The front solution corresponds to a heteroclinic trajectory connecting the equilibria $u = u_s^{\pm}$. The heteroclinic connection exists only at unique value of c (see Fig. 6); thus, the propagation speed is determined uniquely by solving a nonlinear eigenvalue problem. Its value is proportional to the difference of potentials of the two HSS:

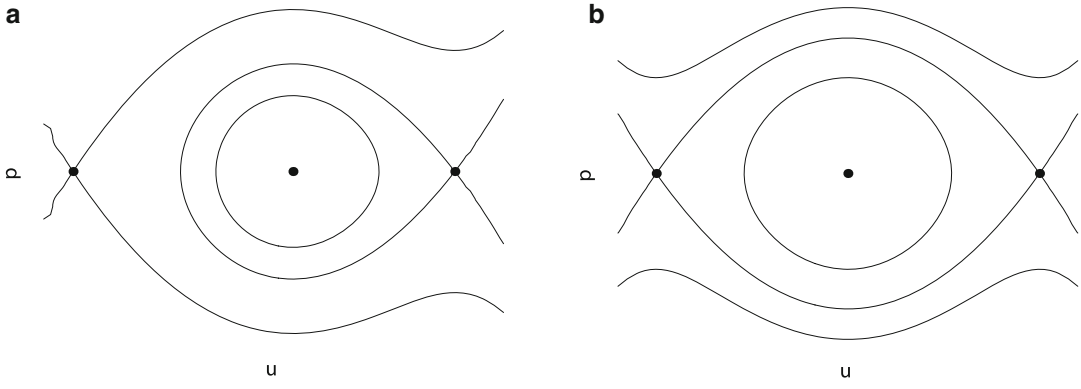

Patterns and Interfaces in Dissipative Dynamics, Fig. 6 Generic trajectories in the phase plane $u, p = u'(x)$ (**a**) and a nongeneric set of trajectories containing a heteroclinic orbit (**b**)

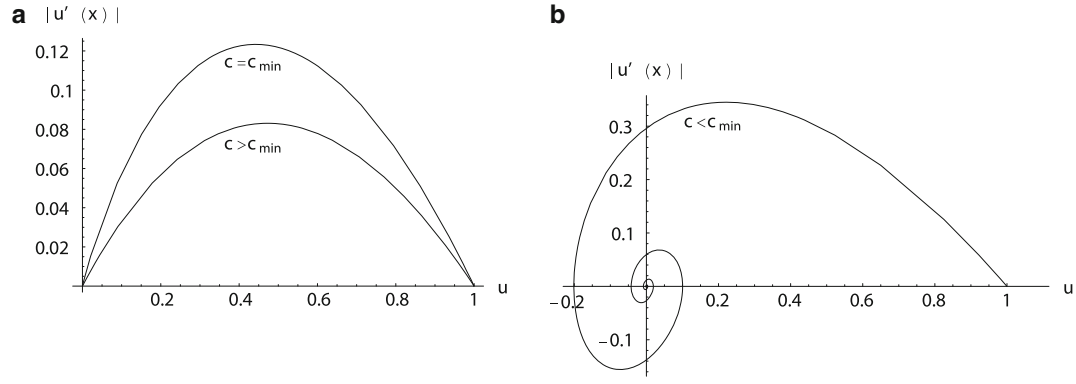

Patterns and Interfaces in Dissipative Dynamics, Fig. 7 Trajectories in the phase plane connecting a stable and an unstable equilibrium

$$c = \frac{D}{\sigma}\Delta V, \quad \Delta V = V\left(u_s^-\right) - V\left(u_s^+\right). \qquad (14)$$

The situation is different when the retreating state $u = u_s^0$ is unstable. This often happens in population dynamics: a state where a competitively advantageous specie is absent is formally unstable to infinitesimal perturbations but will be nevertheless preserved at any location until this specie is introduced there. An unstable state, viewed as an equilibrium point of (13), is a stable node at propagation speeds exceeding a certain threshold $c_{\min}$, Thus, a trajectory starting from the advancing stable HSS connects generically to u_s^0 at any $c > c_{\min}$ (see Fig. 7). Actual propagation speed is selected dynamically at the leading edge (Kolmogorov et al. 1937; van Saarloos 2003), and turns out to be equal to the minimum speed $c_{\min}$, which corresponds to the steepest front profile. Under certain conditions (when overshoots are allowed) a faster speed corresponding to a still steeper profile is selected nonlinearly (van Saarloos 2003). In the former case, the front is "pulled" by perturbations growing at the leading edge and described by linearized equations, while in the latter case, it is "pushed" by nonlinear interactions favoring the advancing state.

Interfacial Instabilities

The front solution is neutrally stable to translations along the x-axis. This neutral (Goldstone) mode is weakly perturbed when the translation is weakly nonuniform, so that the front becomes curvilinear but the curvature radius still far exceeds the characteristic front thickness.

Propagation of a weakly curved front is best understood in a coordinate frame aligned with its deformed shape. The nominal front position is defined by replacing a diffuse transitional region by a planar curve $\mathcal{C}$ drawn along some intermediate level of the variable u. The coordinate lines $x =$ const are obtained by shifting the curve along the normal by a constant increment, as shown in Fig. 8. This shift causes the length to increase on convex, and to decrease on concave side of the curve. Eventually, a singularity develops in the latter direction, but, when the curvature radius is much larger than the characteristic front thickness, this will happen far away within the region where one of the HSS is approached.

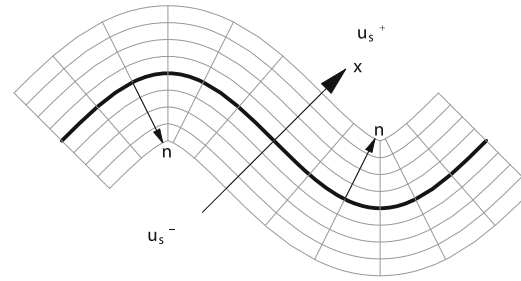

Patterns and Interfaces in Dissipative Dynamics, Fig. 8 Construction of the aligned coordinate frame. The coordinate lines are shown in *gray*. *Arrows* show the local directions of the normal **n** and the *x*-axis. Observe a singularity developing on the concave side

When (13) is rewritten in the aligned frame an expanded viewing the curvature as a small parameter, the local normal propagation speed of a curved front is expressed by the eikonal equation

$$c = c_0 - D\kappa = \frac{D}{\sigma}(\Delta V - \sigma\kappa), \qquad (15)$$

where c_0 is the speed of a planar front and k is the Gaussian curvature.

Since convex front segments propagate slower and concave segments faster, the front tends to flatten, provided c_0 is uniform everywhere. Instabilities may arise, however, when c_0 increases ahead of the front. This may happen in the presence of an externally imposed gradient, as in directional solidification (Langer 1980), but most commonly is caused by an additional "control" field. The control field responsible for the Mullins-Sekerka instability of solidification fronts (Langer 1980; Mullins and Sekerka 1963) is the concentration of a contaminant, which is rejected by the solid and slows down solidification by lowering the melting temperature. Since the contaminant diffuses away more easily from convex segments, they tend to propagate faster, which causes instability when the driving is strong enough to overcome surface tension.

Another example is instability of a combustion front, which separates hot burnt-out and cold fuel-rich domains (Zeldovich 1985). A thin front

structure arises in this case because combustion requires both fuel and sufficient temperature for its initiation, and both fuel concentration and temperature play the role of control variables. When heat transfer is the limiting factor, convex segments cool down and propagate slower, and the front is stable. When, on the opposite, propagation is limited by fuel supply, convex segments accelerate and instability sets on, leading to corrugated fronts.

Dynamics of weak deviations $\zeta(\boldsymbol{y})$ from a stable planar front spanned by a 2-vector y is described by expanding the normal propagation speed, front curvature and the control field in powers of a small parameter scaling both the deviation ζ and its transverse derivative $\nabla_{\mathbf{y}}$, as well as time. For stable fronts, the appropriate scaling is $\zeta = O(1)$, $\nabla_{\mathbf{y}} = O(\in)$, $\partial_t = O(\in^2)$, leading to the Burgers equation

$$\partial_t \zeta = D\nabla_{\mathbf{y}}^2 \zeta - \frac{1}{2} c_0 \left|\nabla_{\mathbf{y}} \zeta\right|^2. \tag{16}$$

The particular coefficients here correspond to (15), but also in other cases the same universal form can be obtained after the coefficients are removed by rescaling, provided the effective diffusivity D is positive. If the latter is negative but small, $|D| = O(\epsilon^2)$, the appropriate scaling is $\zeta = O(\in)$, $\nabla_{\mathbf{y}} = O(\in)$, $\partial_t = O(\in^4)$, and expanding to a higher order yields, after scaling away the coefficients, the Kuramoto-Sivashinsky equation (Sivashinsky 1977)

$$\partial_t \zeta + \nabla_{\mathbf{y}}^2 \zeta + \left(\nabla_{\mathbf{y}}^2\right)^2 \zeta + \frac{1}{2}\left|\nabla_{\mathbf{y}} \zeta\right|^2 = 0. \tag{17}$$

This equation, appearing also in phase dynamics (Kuramoto and Tsuzuki 1976), is a paradigm of weak turbulence.

Front Interactions and Coarsening

Fronts of opposite polarity in a one-dimensional system attract and eventually coalesce, thereby coarsening the distribution of domains, which may have been created initially in the process of phase separation or relaxation to alternative HSS. The interaction is, however, very weak, falling off exponentially with separation. In higher dimensions, the principal cause of coarsening, or Ostwald ripening, is the curvature dependence of the propagation speed, whereby small droplets with high curvature tend to shrink and eventually disappear. This is a manifestation of the Gibbs-Thomson effect relating the equilibrium conditions with the radius of a droplet.

Coarsening most often occurs under conditions when evolution is constrained by a conservation law, so that the integral $\int u(\mathbf{x})\mathrm{d}\mathbf{x}$ expressing the total amount of material in the system remains constant. Under these conditions, fronts cannot move independently from each other. The conservation law is accounted for when (11) is replaced by the Cahn-Hilliard equation (Cahn and Hilliard 1958)

$$\partial_t u = \nabla^2 \mu, \quad \mu = -\left[D\nabla^2 u + f(u)\right]. \tag{18}$$

The eikonal equation governing the front motion retains the form (15), but the value c_0 depends on chemical potential μ. The latter shifts in the course of coarsening in such a way that the value of the critical radius $R = \kappa^{-1}$ of a droplet that neither grows or shrinks, keeps growing as smaller droplets disappear. Analytical theory (Lifshitz and Slyozov 1958) predicts universal asymptotic droplet size distribution at late stages of coarsening.

Structures Built up of Fronts

Coarsening can be precluded when changes in an additional control field arrest growth of large and shrinking of small domains. This leads to formation of a variety of patterns and solitary structures. The paradigmal system for exploring these phenomena is the FitzHugh-Nagumo system, which has the form (1), (2) with the function $f(u, v)$ cubic in u and linear in v and a linear function $g(u, v)$. The rescaled form suitable for the analysis of stationary structures is

$$\in^2 \partial_t u = \in^2 \nabla^2 u + u - u^3 - \in v, \tag{19}$$

$$\tau^{-1} \partial_t v = \nabla^2 v - v - v + \mu u, \tag{20}$$

Here $\in = \sqrt{\gamma_1 D_1 / \gamma_2 D_2} << 1$ is the ratio of the characteristic lengths associated with the

activator and the inhibitor, $\tau = D_2/D_1$; the small coupling parameter ε in (19) ensures a balance between the effect of small interfacial curvature and weak symmetry breaking between the alternative HSS $u_s^{\pm} = \pm 1 + O(\in)$; the remaining parameters μ and ν regulate the coupling stress and bias.

Structures generated by the system (19), (20) are built up by assigning a region where the activator approaches one of the alternative HSS, computing the respective inhibitor distribution, and finding stationarity conditions for the fronts forming the boundaries of this region (Ohta et al. 1989). Possible stationary structures in two dimensions are a solitary band, a solitary disk, a striped pattern, or a hexagonal grid consisting of almost circular spots. The size of spots or stripes is determined by the parameters of the system, but there is a considerable leeway in choosing the general configuration. Under certain conditions, it even might be possible to store information by creating or extinguishing spots at chosen locations (Coullet et al. 2004). In other cases, splitting of a solitary spot initiates a multiplication cascade (Reynolds et al. 1994), leading eventually to a hexagonal pattern filling the plane.

Instabilities of stationary structures are studied with the help of the linearized eikonal equation (15) combined with the inhibitor equation (20) where the last term is expressed through a shift of the front position. Both solitary bands and disks can suffer zigzag (leading eventually to splitting), oscillatory and traveling instabilities. The latter two become prevalent as the parameter τ decreases, so that the inhibitor response to front displacements slows down. For example, a solitary band is destabilized in the zigzag mode at $\tau > 1$, while the traveling instability comes first at smaller τ (see Fig. 9). Oscillatory instability is always preceded by traveling one in this case, but may become relevant for a solitary disk.

Traveling instability indicates transition to various propagating structures and wave patterns. A solitary spot tends to either dissolve or spread out sidewise after being immobilized; in the latter case, a spiral structure starts to develop as the ends lag behind. A traveling spot can be, however, stabilized if a second inhibitor, both fast and long-range, is added (Or-Guil et al. 1998).

Various patterns of propagating fronts can be generated beyond this limit by the same FitzHugh-Nagumo system, which, however, should be scaled differently for this purpose. Unlike stationary or slowly evolving patterns where the characteristic length scale is set by the diffusional range of the long-scale inhibitor, the wavelength of a propagating pattern is tied to the propagation speed and remains finite even when the inhibitor is nondiffusive.

The long scale should be redefined therefore on the basis of the characteristic propagation speed of the activator front $c^* = \sqrt{D_1/\gamma_1}$ and the characteristic relaxation time of the inhibitor γ_2. Using this "advective" length unit, $L^* = \gamma_2\sqrt{D_1/\gamma_1}$ brings (1), (2) to the dimensionless form

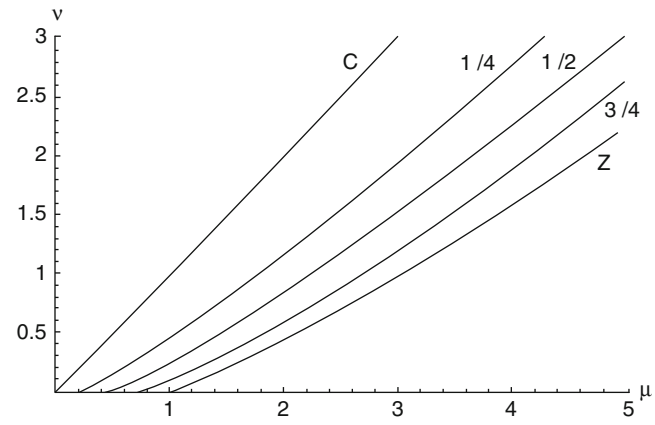

Patterns and Interfaces in Dissipative Dynamics, Fig. 9 Existence boundary (*C*) and loci of zigzag (*Z*) and traveling instability for a solitary band. The loci of traveling instability are marked by respective values of τ. A stable band exists between the line C and an applicable instability locus

$$\gamma \partial_t u = \gamma^2 \nabla^2 u + f(u, v), \tag{21}$$

$$\partial_t v = \delta^2 \nabla^2 v + g(u, v), \tag{22}$$

where $\gamma = \gamma_1/\gamma_2, \delta = \gamma/\in = \sqrt{\gamma D_2/D_1}$ .The "inner" scale of the transitional layer, where the system switches between the two alternative activator states, $u = u_s^{\pm}$, is now set exclusively by the capacitance ratio γ, independently of diffusivities, and, provided $\gamma \ll 1$, remains small even when the inhibitor is less diffusive than the activator. The parameters can be chosen in such a way that $\delta \ll 1$, so that the inhibitor diffusion is negligible, provided $\gamma \ll D_1/D_2$. Under these conditions, the inhibitor diffusion can be neglected, reducing (22) to $\partial_t v = g(u, v)$. Although this equation contains no mechanism for healing discontinuities in v, the inhibitor field should remain smooth in the course of evolution, barring freaky initial conditions or strongly localized perturbations. This opens the easiest way of constructing various wave patterns, including such exotic objects as chaotic wave trains (Elphick et al. 1988).

Interfaces of Patterns

Interfaces between different patterns or different pattern orientations (domain walls) can be described in the simplest way on the level of amplitude equations. This may give qualitatively correct results in static problems, even though changes across a domain wall in patterns generated in simulations and experiments are usually effected on a length comparable with the prevailing wavelength of the pattern. One can expect that a stationary solution exists only when the wavelengths are equal on both sides of the wall; otherwise, the wall would propagate in the direction decreasing the overall energy of the pattern. It turns out that an even stronger restriction is true, and both wavelengths should be optimal (Malomed et al. 1990). In this way, domain walls, alongside dislocations, enhance relaxation of the pattern to the optimal wavelength.

Dynamic problems are strongly influenced by detailed structure of the pattern, which is lost on the level of amplitude equations. When a pattern advances into an unstable uniform state, the wavelength selected at the leading edge is not identical to the wavelength of the full-grown pattern formed behind the front, and neither one coincides with the optimal wavelength (Ben-Jacob et al. 1985).

In the case when a stable homogeneous solution coexists with a stable periodic pattern, stable stationary fronts between the two states exist within a finite parametric interval (Pomeau 1986), rather than at a single point where the energies of both states are equal, as amplitude equations would predict. The motion of this front is affected by the discrete structure of the pattern, which causes self-induced pinning hindering the retreat of a metastable state. There are two depinning transitions, corresponding to "crystallization" or "melting" of the pattern, shown schematically by thick lines in Fig. 10. Between the two limits, various metastable stationary structures exist: a single cell ("soliton"), a finite patterned inclusion, sandwiched between semi-infinite domains occupied by a uniform state, or a semi-infinite pattern, coexisting with a uniform state. To the right of the crystallization threshold C, the pattern advances by a periodic nucleation process which creates new elementary cells at the interface (Aranson et al. 2000), while to the left of the melting limit M, the pattern recedes as elementary cells at the interface are destroyed. A different, far more efficient depinning mechanism works in two dimensions (Hagberg et al. 2006). It is initiated by a zigzag instability of the pattern followed by nucleation of disclinations, which further move toward the uniform state, as seen in Fig. 11. This generates stripes extending in the normal direction, turning eventually the original boundary into a domain wall separating striped patterns rotated by $\pi/2$.

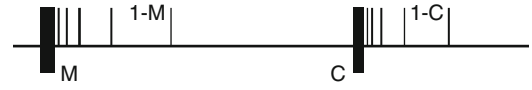

Patterns and Interfaces in Dissipative Dynamics, Fig. 10 A scheme of depinning transitions showing crystallization (*C*) and melting (*M*) thresholds for an infinite cluster, as well as the corresponding limits for clusters of different sizes, terminating in single-cell limits 1-C, 1-M

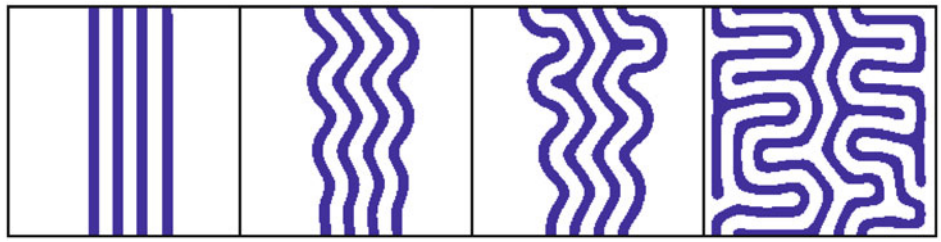

Patterns and Interfaces in Dissipative Dynamics, Fig. 11 Depinning of striped pattern initiated by a zigzag instability (Hagberg et al. 2006)

Wave Patterns

Plane Waves

A simplest propagating wave pattern is a periodic solution depending on a moving coordinate $\xi = x - ct$, where $c = \omega/k$ is phase velocity, ω is frequency and k is wavenumber. A waveform ~ exp. [i($kx - \omega t$)] may emerge directly by symmetry breaking bifurcation, but this is not the most common mechanism. It is impossible, in particular, in a two-component RDS (1), (2), where other scenarios lead to wave patterns. One of them, mentioned in the preceding section, is traveling instability of stationary structures. Another road to wave patterns, most amenable to analytical tools, starts in the vicinity of a Hopf bifurcation, where small-amplitude oscillations weakly modulated in space are described by the complex Ginzburg-Landau (CGL) equation. Its standard rescaled form is

$$\partial_t u = (1 + i\eta)\nabla^2 u + u - (1 + iv)|u|^2 u. \quad (23)$$

A plane wave solution of (23) with the wave vector $\boldsymbol{k}$ is

$$\begin{aligned} u &= \rho_0 \exp[i(\boldsymbol{k}\cdot\boldsymbol{x} - \omega t)], \\ \rho_0 &= \sqrt{1-k^2}, \quad \omega = v + (\eta - v)k^2. \end{aligned} \quad (24)$$

The waves are dispersive, and the group velocity is $\boldsymbol{v} = 2\,\boldsymbol{k}(\eta - v)$.

Instabilities of plane waves are studied most efficiently with the help of the phase dynamics approach, since the most dangerous perturbation modes can be viewed as long-scale distortions of neutrally stable translational modes. The longitudinal and transverse phase diffusivities are

$$D_{\|} = \frac{1 + v\eta - k^2(3 + v\eta + 2v^2)}{1 - k^2}, \quad D_{\perp} = 1 + v\eta. \quad (25)$$

Vanishing $D_{||}$ marks the threshold of Eckhaus instability, which limits the range of stable wavenumbers. Vanishing $D_{\perp}$ signals Benjamin-Feir (self-focusing) instability, independently of the wavelength. Both instabilities arising at the respective thresholds are convective, which means that growing perturbations are washed away with the prevailing group velocity. The absolute instability condition stipulating growth of perturbation at a particular location is less restrictive (see Fig. 12). Numerical simulations (Aranson and Kramer 2002) show that transition to turbulence occurs only when the absolute stability condition is violated, but the system is very sensitive to noise in the convectively unstable region.

Besides uniform wave trains, there is a variety of non-uniform one-dimensional solutions of the CGL equation with a constant frequency and spatially varying modulus and wavenumber, which are stationary in a frame propagating with a certain speed c and depend on the comoving coordinate $\xi = x - ct$ only. The solutions approaching asymptotically at $\xi \to \pm\infty$ either plane waves or the trivial state can be also viewed as defects separating domains where different uniform states prevail. Such solutions include pulses, approaching the trivial state at both extremes; nonlinear fronts, separating the trivial state from an invading wave train, and domain boundaries separating plane waves directed in the opposite

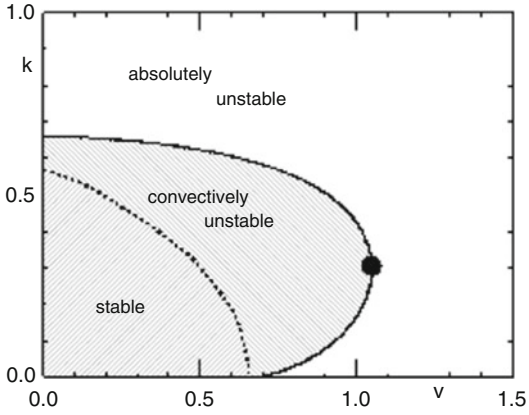

Patterns and Interfaces in Dissipative Dynamics, Fig. 12 Limits of convective and absolute instabilities in the plane (v, k) for $\eta = -3/2$. The *dot* marks the limit of convectively unstable waves (Aranson and Kramer 2002, reproduced with permission. Copyright by the American Physical Society)

sense and, possibly, having different wavelength (Aranson and Kramer 2002; van Saarloos and Hohenberg 1992). Interactions among various defects dominate chaotic dynamics beyond the self-focusing instability limit (Brusch et al. 2001).

Amplitude equations for wave patterns emerging directly from an HSS through a symmetry breaking bifurcation with $\omega \neq 0$, $k \neq 0$ should account for competition between waves with amplitudes $u^{\pm}$ propagating in the opposite directions, which may either suppress one another or combine to a standing wave. The normalized form of coupled equations for $u^{\pm}$ is

$$\begin{aligned}\partial_t u^{\pm} \pm c u_x^{\pm} &= (1+\mathrm{i}\eta) u_{xx}^{\pm} + u^{\pm} \\ &\quad - (1+\mathrm{i}v_+)\left|u^{\pm}\right|^2 u^{\pm} \\ &\quad - g(1+iv_-)|u^{\mp}|^2 u^{\pm}, \end{aligned} \tag{26}$$

where g is a coupling parameter. The orders of magnitude of all terms of these equations can be balanced only when the phase velocity $c = \omega/k$ is of the same $O(\epsilon)$ as $u^{\pm}$. Genetically, $c = O(1)$, and the advective term $cu_x^{\pm}$ is dominant. For a single wave, it can be removed by transforming to the comoving frame. When both waves are present, each wave, viewed in its own frame $\xi_{\pm} = x \mp ct$ samples the average amplitude of its counterpart propagating in this frame with a fast speed. The appropriate amplitude equations have then the form (Knobloch and de Luca 1990)

$$\begin{aligned}\partial_t u^{\pm} &= (1+\mathrm{i}\eta) u^{\pm}_{\xi_{\pm}\xi_{\pm}} + u^{\pm} \\ &\quad - (1-\mathrm{i}v_+)\left|u^{\pm}\right|^2 u^{\pm} \\ &\quad - g(1+\mathrm{i}v_-)|u^{\mp}|^2 u^{\pm}. \end{aligned} \tag{27}$$

These equations retain only global coupling carried by the spatial averages $\langle |u^{\mp}|^2 \rangle$.

In two dimensions, the amplitude equations also involve resonant interactions of pairs of waves propagating in the opposite directions. This makes possible complex dynamics even when the amplitudes are uniform and obey space-independent equations (Pismen 1986)

$$\begin{aligned}&\partial_t u_1^+ \\ &= u_1^+\left[\mu - v_+|u_1^+|^2 - v_-|u_1^-|^2 - \beta\left(|u_2^+|^2 + |u_2^-|^2\right)\right] \\ &\qquad + \overline{\gamma u_2^-}\, u_2^+ u_2^- . \end{aligned} \tag{28}$$

Spiral and Scroll Waves

A ubiquitous and extensively studied waveform is a rotating spiral wave. Its specific feature is the presence of a phase singularity. An n-armed spiral wave can be constructed as a circularly symmetric vortex solution of (23) with the topological charge n, i.e. phase circulation $2\pi n$. Unlike a symmetric defect in (8), the phase must also depend on the radial coordinate, so that the vortex radiates a wave with a certain uniquely selected asymptotic wavenumber k_∞. This solution is obtained (Hagan 1982) in polar cooordinates r, ϕ by assuming an *ansatz*

$$u = \rho(r)\mathrm{e}^{\mathrm{i}\theta}, \quad \theta = n\boldsymbol{\phi} + \psi(r) - \omega t. \tag{29}$$

Using this *ansatz* brings (23) to the form

$$\begin{aligned}&\rho''(r) + r^{-1}\rho'(r) \\ &\quad + \left(1 - k^2 - n^2/r^2 - \rho^2\right)\rho \\ &\quad = 0, \end{aligned} \tag{30}$$

$$\frac{1}{r\rho^2}\frac{\mathrm{d}}{\mathrm{d}r}\left(rk\rho^2\right) = q\left(\rho_\infty^2 - \rho^2\right), \tag{31}$$

where $k = \psi'(r)$ is the radial wavenumber. Stability analysis of plane waves applies also to far

regions of spiral waves; one could expect therefore a transition to a turbulent state to occur under conditions when the selected asymptotic wavenumber k_∞ falls into the range where the corresponding plane wave solution of (23) is unstable. The respective stability limits in the parametric plane (η, ν) are presented in Fig. 13.

Another approach to constructing rotating spiral waves exploits kinematics of fronts of opposite polarity described by RDS (21), (22) (Tyson and Keener 1988). The inhibitor diffusion can be neglected almost everywhere, except in the crucial tip region where the two fronts meet. Behavior of the spiral tip and its meandering instability has been elucidated analytically using a multiscale technique matching different approximations in overlapping regions (Hakim and Karma 1999). Complex dynamics of a meandering tip, which exhibit quasiperiodic and chaotic motion in some parametric domains, can be well described with the help of a simpler phenomenological model (Barkley 1994). A similar instability of spiral waves described by the CGL equation is the core acceleration instability (Aranson and Kramer 2002), which may serve as a trigger of transition to spatio-temporal chaos alternative to instability of radiated waves.

A special kind of spiral wave patterns arises when the underlying dynamical system undergoes a period doubling transition. The period doubling causes the appearance of synchronization defect (SD) lines, which serve to reconcile the doubling of the oscillation period with the period of rotation of the spiral wave (see Fig. 14a). These lines are defined as the loci of those points in the medium where the two loops of the period two orbit exchange their positions in local phase space. The period two oscillations on the opposite sides of a SD are shifted relative to each other by 2π (i.e., a half of the full period), so that the dynamics projected on the rotation direction is effectively of period one, while it is of period two locally at any point in the medium (Fig. 14b).

A three-dimensional extension of a rotating spiral is a rotating scroll wave. The core filament of a scroll wave is a line vortex. A scroll wave with a straight-line core directed along the z-axis has identical spiral waves in each cross-section. Even then, the structure can be nontrivial if the spiral phases are given a phase twist, i.e. are

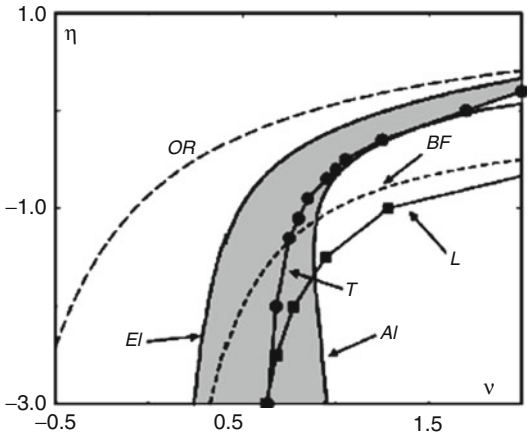

Patterns and Interfaces in Dissipative Dynamics, Fig. 13 Stability limits of a spiral wave solution in the parametric plane (η, ν). The curve *EI* shows the limit of convective instability and *AI*, of absolute instability for the waves emitted by the spiral; *OR* is the boundary of the oscillatory spatial decay for the emitted waves, $q = 0.845$ (bound states exist to the right of this line). *BF* indicates the Benjamin-Feir limit $\nu\eta = -1$, *L* is the limit of phase turbulence, and *T* corresponds to the transition to defect turbulence for random initial conditions (Aranson and Kramer 2002, based on Chaté and Manneville 1996; reproduced with permission. Copyright by the American Physical Society)

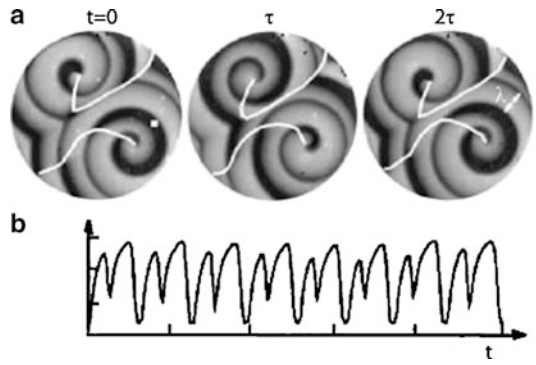

Patterns and Interfaces in Dissipative Dynamics, Fig. 14 (**a**) A pair of period two spiral waves with the fundamental period τ and the average wavelength λ. The *white solid lines* are the synchronization defects. (**b**) A period two time series measured at the point marked by the *white filled square* (Park and Lee 2002, reproduced with permission. Copyright by the American Physical Society)

shifted along the z-axis. A curved core filament may also close up into a ring or even form knots. A stable scroll structure evolves to decrease the filament curvature (Keener 1988). This kind of dynamics is similar to curvature-driven motion of interfaces, but may be reversed when the filament is unstable. The most dangerous perturbation modes are long-scale modes associated with meandering or translational core deformations (Henry and Hakim 2002). Meandering instability usually saturates as a distorted scroll wave with a twisted rotating core (Fig. 15). Instability in the translation mode, which causes spontaneous bending of the scroll axis, does not saturate, but gives rise to a scroll wave with a continuously extending core (Fig. 16a). This leads to a turbulent state visualized as a tangle of breaking wave fronts (Fig. 16b).

Spiral Patterns and Turbulence

Interaction of spiral waves is dominated by shocks – domain boundaries where waves emanating from different centers collide. The shocks effectively screen different spiral domains from radiation emitted by other spiral cores. A typical example of a spiral domain pattern in a stable parametric range obtained in a CGL simulation run starting from random initial conditions (Chaté and Manneville 1996) is shown in Fig. 17. At the initial stage, the system tends to relax locally to the stable state with unity real amplitude, but, as the phases are random, the relaxation is frustrated,

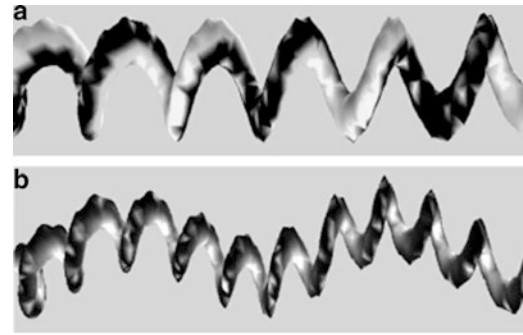

Patterns and Interfaces in Dissipative Dynamics, Fig. 15 (**a**) A restabilized helical vortex; (**b**) A doubly periodic "superhelix" Isosurfaces of the modulus $\rho = 0.6$ shaded by phase field are shown (CGL simulations (Rousseau et al. 1998), reproduced with permission. Copyright by the American Physical Society)

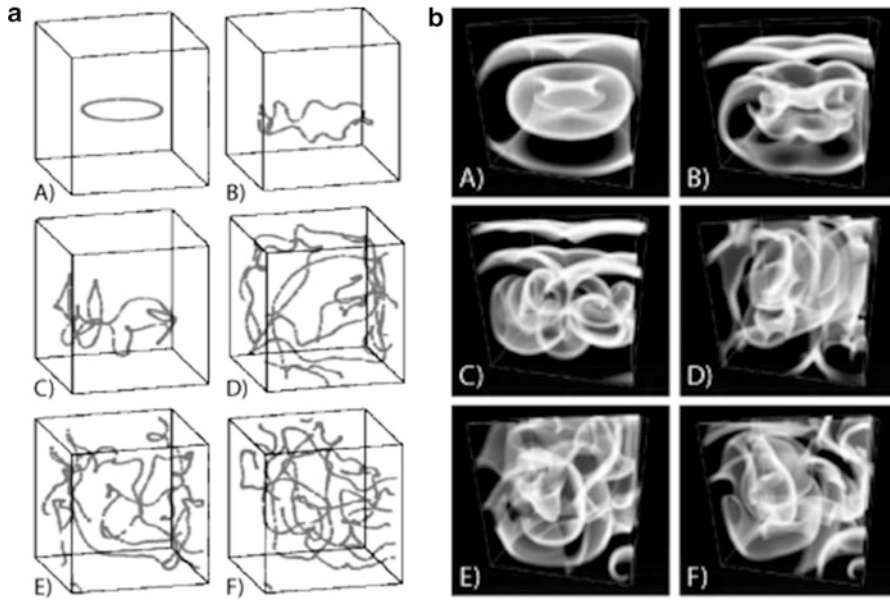

Patterns and Interfaces in Dissipative Dynamics, Fig. 16 Transition to turbulence due to core filament extension and breakup of scroll waves. (**a**) Snapshots of the core filament, starting from a closed loop. (**b**) Respective snapshots of wave patterns showing semitransparent visualization of the activator fronts (Alonso et al. 2004, reproduced with permission. Copyright by the American Physical Society)

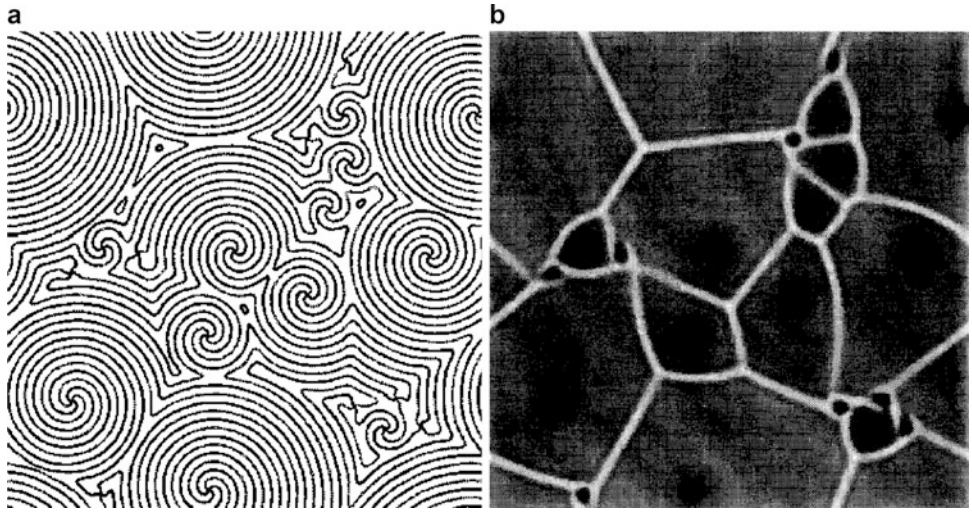

Patterns and Interfaces in Dissipative Dynamics, Fig. 17 Spiral domains. *Left:* levels of constant phase. *Right:* grayscale amplitude map showing enhanced amplitudes at the shocks (CGL simulations (Chaté and Manneville 1996), reproduced with permission from Elsevier Science)

and a large number of defects – vortices of unit charge – are formed. At the following coarsening stage, oppositely charged vortices annihilate, so that the density of defects decreases. The coarsening process, however, stops halfway, leaving a certain number of single-charged spiral vortices with either sense of rotation. Vortices that failed to conquer a sufficiently large domain are reduced to "naked cores", left to satisfy the topological condition of conservation of circulation. The resulting stable spiral domain pattern is called vortex glass. The waves always propagate outwards from the vortex cores, so that the entire domain structure is generated when local order spreads out from centers to the periphery. Perturbations, also traveling outwards with the prevailing group velocity, are absorbed at shocks, and therefore the pattern may survive beyond the convective instability threshold. The turbulent state takes over only when the emanated waves become absolutely unstable, i.e., when some perturbations grow locally in the laboratory frame.

The overall structure of the pattern changes in the range of oscillatory spatial decay of waves emanated by the spiral cores (below the line OR in Fig. 13). Under these conditions, formation of stable bound spiral pairs becomes possible (see Fig. 18). Unlike the monotonic range, spiral domains may have in oscillatory range a wide size distribution, since shocks can be immobilized at different separations.

"Frozen" glassy patterns actually evolve on a very long time scale, as revealed in very long simulation runs (Brito et al. 2003). In the monotonic range, spiral cores perform very slow diffusive motion; the apparent diffusivity increases with vortex density. In contrast, in the oscillatory range, spiral population spontaneously segregates after a very long transient into two distinct phases: large and almost immobile spirals and clusters of trapped small vortices. When the "liquid fraction" is small, the resulting pattern exhibits slow intermittent dynamics: bursts of activity separated by long quiescent intervals. The system keeps evolving on an extremely slow scale, which is consistent with exponentially weak repulsion between well separated spiral cores.

Another possibility, realized in a different parametric region, is a dynamic chaotic state that shows no persistent features. This state is attained under conditions when either spiral waves or vortex cores, or both, are unstable. One can distinguish between mild phase turbulence when no phase singularities occur, and defect chaos characterized by persistent creation and annihilation of vortex pairs. Phase turbulence may persist in the

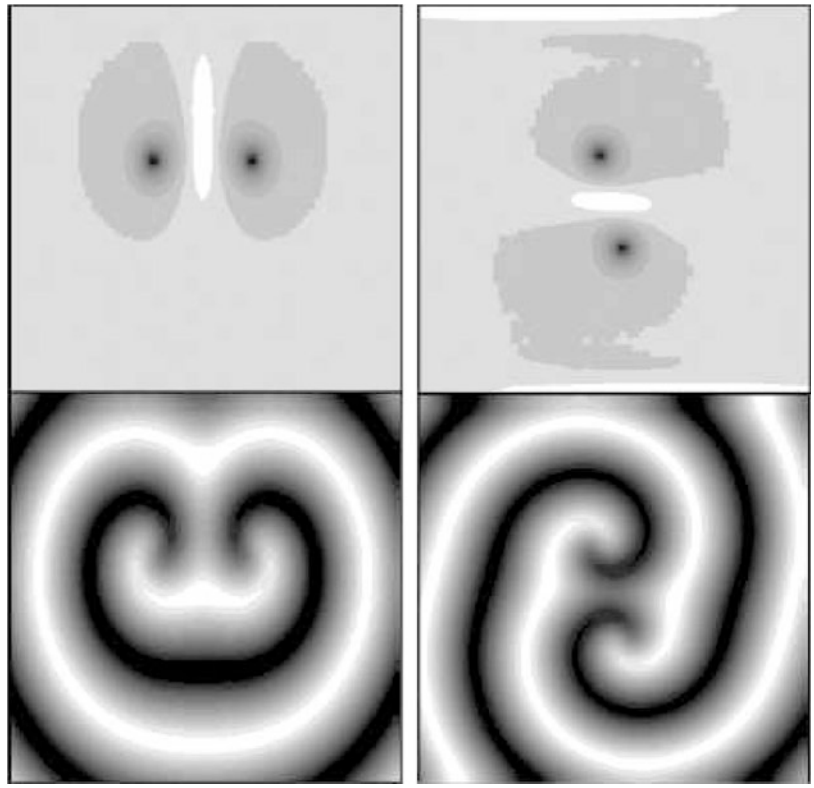

Patterns and Interfaces in Dissipative Dynamics, Fig. 18 Bound states of oppositely (*left*) and likely (*right*) charged spirals (CGL simulations, $\eta = 0$, $\nu = 1.5$). The images show the modulus $\rho(x, y)$ (*top*) and Re(u) (*bottom*) (Aranson and Kramer 2002, reproduced with permission. Copyright by the American Physical Society)

parametric region between the Benjamin-Feir line and the line L in Fig. 13 (Chaté and Manneville 1996). Beyond the line L, defects are created spontaneously, leading to defect chaos. Transition from vortex glass to defect turbulence in simulations starting from random initial conditions occurs at the numerically determined line T in Fig. 13 (Chaté and Manneville 1996). The transition occurs somewhat prior to the absolute instability limit determined by the linear stability analysis of plane waves emitted by spirals. This limit can be approached, however, by starting from carefully prepared initial conditions in the form of large spirals. Prior to the transition, one can observe transient defect turbulence which is unstable to spontaneous nucleation of spirals from the "turbulent sea", leading eventually to a vortex glass state.

Forced Systems

External forcing, including spatially as well as temporally variable inputs, can be used in a straightforward way to enhance or suppress spontaneously emerging patterns (Nepomnyashchy et al. 2004). Alternatively, it may enhance complexity by introducing additional spatial and temporal resonances, which may lead to formation of quasicrystalline structures (Pismen 1987). Resonant forcing of oscillatory systems may drastically change the structure of wave patterns through phase locking. This happens when the CGL equation is forced on a frequency ω_c commensurate with the basic frequency ω_0 at the Hopf bifurcation. For an integer ratio $\omega_c/\omega_0 = n$, the amplitude equation amending (23) can be written by adding the forcing term possessing the required symmetry:

$$\partial_t u = (1 + \mathrm{i}\eta)\nabla^2 u + (\mu + \mathrm{i}\omega)u - (1 - \mathrm{i}\nu)|u|^2 u + \gamma u^{-n-1}, \qquad (32)$$

where γ is the forcing amplitude and $\epsilon^2\omega$ is weak effective detuning, due to both parametric deviations from the Hopf bifurcation point and weak mismatch between ω_c/n and ω_0. The forcing term breaks the symmetry of the CGL equation to phase rotations, reducing it to discrete symmetry $u \to \mathrm{e}^{i\pi m}u$, $m = 1$, $\ldots$, $n - 1$. This changes

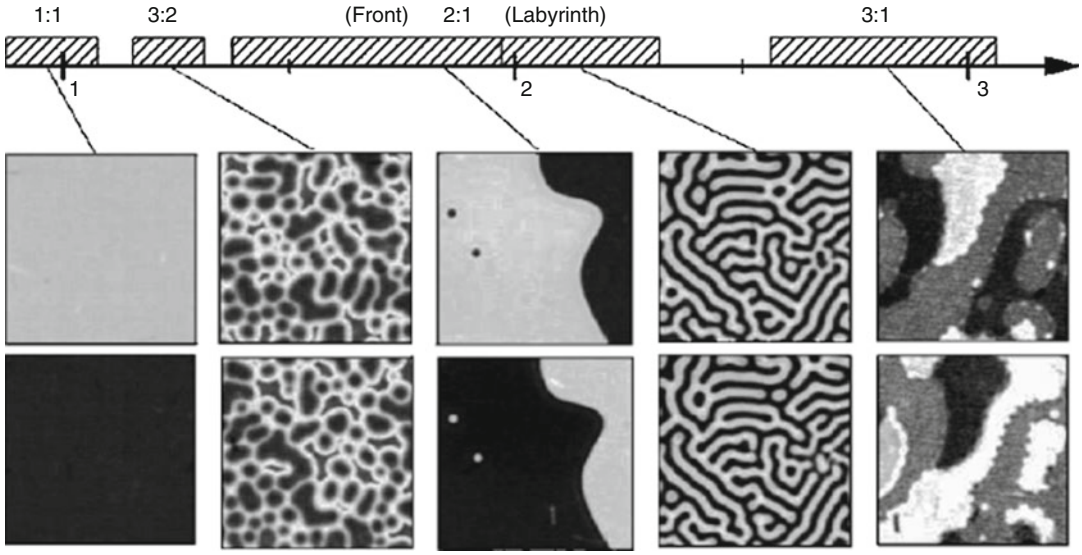

Patterns and Interfaces in Dissipative Dynamics, Fig. 19 Frequency-locked regimes (experiment with light-sensitive reaction under periodic optical forcing [*71*], reproduced with permission). The *axis above* shows the ratio of the forcing to basic frequency. Patterns are shown in pairs, one above the other, at times separated by the forcing period $2\pi/\omega_c$,except for the 1:1 resonance where the interval is π/ω_c

the character of defects: instead of vortices, one can observed fronts separating alternative phase states.

Various patterns at different forcing frequencies, which can be modeled by (32), were observed both in experiments and simulations (Petrov et al. 1997; Lin et al. 2004). Some typical patterns are shown in Fig. 19. For the case of strong resonance ($n = 1$), this system provides a convenient tool for studying transitions between stationary and propagating fronts (Coullet and Emilsson 1992), labyrinthine patterns (Yochelis et al. 2004), and solitary structures (Gomila et al. 2007). These structures are not unlike those observed in the FitzHugh-Nagumo system, although they represent standing waves with the alternative phases interchanging within each domain. Higher resonances create still more complex dynamics involving interactions of different kinds of fronts (Gallego et al. 2001).

Future Directions

The study of pattern formation is now a mature discipline based on well-established general theory and wealth of experimental evidence. The center of attention is turning to specific applications; among them, nonlinear optics and studies of granular media come to the forefront. Forcing and control of patterns, either enhancing or suppressing the complexity of behavior, are studied in detail. As a humble laptop turns into a supercomputer, more fascinating patterns, envy of abstract expressionists, are generated by model equations of increased complexity. Patterns showing dazzling mix of order and chaos are seen as well in various experimental setups.

The ultimate aim of controlled creation of self-organized structures still remains elusive, and new ideas are awaited as the new century comes of age. The study of pattern formation, dealing with ubiquitous problems of order and chaos, is bound to find its way into basic curricula and wealth of practical applications.

Bibliography

Primary Literature

Abou B, Wesfreid JE, Roux S (2000) J Fluid Mech 416:217
Alexander S, McTague J (1978) Phys Rev Lett 41:702

Alonso S, Kähler R, Mikhailov AS, Sagués F (2004) Phys Rev E 70:056201
Aranson IS, Kramer L (2002) Rev Mod Phys 74:99
Aranson IS, Malomed BA, Pismen LM, Tsimring LS (2000) Phys Rev E 62:R5
Arecchi FT (1999) Phys Rep 318:1
Assenheimer M, Steinberg V (1993) Phys Rev Lett 70:3888
Barkley D (1994) Phys Rev Lett 72:164
Bénard H (1900) Ann Chim Phys 7 (Ser 23) 62
Ben-Jacob E, Brand HR, Dee G, Kramer L, Langer JS (1985) Physica D 14:348
Bodenschatz E, Pesch W, Kramer L (1988) Physica D 32:135
Bodenschatz E, Pesch W, Ahlers G (2000) Annu Rev Fluid Mech 32:709
Bowman C, Newell AC (1998) Rev Mod Phys 70:289
Braun E, Steinberg V (1991) Europhys Lett 15:167
Brito C, Aranson IS, Chaté H (2003) Phys Rev Lett 90:068301
Brusch L, Torcini A, van Hecke M, Zimmermann MG, Bär M (2001) Physica D 160:127
Burger M, Field RJ (1985) Oscillations and traveling waves in chemical systems. Wiley, New York
Cahn JW, Hilliard JE (1958) J Chem Phys 28:258
Chaté H, Manneville P (1996) Physica A 224:348
Coullet P, Emilsson K (1992) Physica D 61:119
Coullet P, Riera C, Tresser C (2004) Chaos 14:193
Cross MC, Newell AC (1984) Physica D 10:299
Elphick C, Meron E, Spiegel EA (1988) Phys Rev Lett 61:496
Faraday M (1831) Philos Trans R Soc Lond 121:299
Gallego R, Walgraef D, San Miguel M, Toral R (2001) Phys Rev E 64:056218
Gierer A, Meinhard H (1972) Kybernetik 12:30
Gilad E, Shachak M, Meron E (2007) Theor Popul Biol 72:214
Gomila D, Colet P, San Miguel M, Oppo G-L (2007) Eur Phys J Spec Top 146:71
Hagan PS (1982) SIAM J Appl Math 42:762
Hagberg A, Yochelis A, Yizhak H, Elphick C, Pismen LM, Meron E (2006) Physica D 217:186
Hakim V, Karma A (1999) Phys Rev E 60:5073
Hamley IW (2003) Nanotechnology 14:R39
Henry H, Hakim V (2002) Phys Rev E 65:046235
Josserand C, Pomeau Y, Rica S (2007) Eur Phys J Special Topics 146:47
Keener JP (1988) Physica D 31:269
Knobloch E, de Luca J (1990) Nonlinearity 3:975
Kolmogorov A, Petrovsky I, Piskunov N (1937) Bull Univ Moscow. Ser Int Sec A 1:1
Kuramoto Y, Tsuzuki T (1976) Prog Theor Phys 55:356
Langer JS (1980) Rev Mod Phys 52:1
Lifshitz IM, Slyozov VV (1958) Zh Eksp Teor Fiz 35:479
Lin AL, Hagberg A, Meron E, Swinney HL (2004) Phys Rev E 69:066217
Malomed BA, Nepomnyashchy AA, Tribelsky MI (1990) Phys Rev A 42:7244
Mermin ND (1979) Rev Mod Phys 51:591
Mullins WW, Sekerka RF (1963) J Appl Phys 34:323
Murray JD (1981) J Theor Biol 88:161
Nepomnyashchy AA, Pismen LM (1991) Phys Lett A 153:427
Nepomnyashchy AA, Golovin AA, Gubareva V, Panfilov V (2004) Physica D 199:61
Newell AC, Whitehead JA (1969) J Fluid Mech 38:279
Newell AC, Passot T, Bowman C, Ercolani N, Indik R (1996) Physica D 97:185
Ohta T, Mimura M, Kobayashi R (1989) Physica D 34:115
Or-Guil M, Bode M, Schenk CP, Purwins H-G (1998) Phys Rev E 57:6432
Ouyang Q, Swinney HL (1991) Nature 352:610
Pampaloni E, Residori S, Soria S, Arecchi FT (1997) Phys Rev Lett 78:1042
Park J-S, Lee KJ (2002) Phys Rev Lett 88:224501
Petrov V, Ouyang Q, Swinney HL (1997) Nature 388:655
Pismen LM (1986) Dyn Stab Syst 1:97
Pismen LM (1987) Phys Rev Lett 59:2740
Pismen LM, Rodriguez JD (1990) Phys Rev A 42:2471
Pismen LM, Rubinstein BY (1999) Chaos Soliton Fractal 10:761
Pomeau Y (1986) Physica D 23:3
Pomeau Y, Manneville P (1979) J Phys Lett 40:L609
Proctor MRE, Jones CA (1988) J Fluid Mech 188:301
Rabinovich MI, Tsimring LS (1994) Phys Rev E 49:R35
Reynolds WN, Pearson JE, Ponce-Dawson S (1994) Phys Rev Lett 72:2797
Rousseau G, Chaté H, Kapral R (1998) Phys Rev Lett 80:5671
Sagués F, Sancho JM, García-Ojalvo J (2007) Spatiotemporal order out of noise. Rev Mod Phys 79:829
Segel LA (1969) J Fluid Mech 38:203
Sivashinsky GI (1977) Acta Astronaut 4:1177
Turing AM (1952) Philos Trans R Soc Lond Ser B 237:37
Tyson JJ, Keener JP (1988) Physica D 32:327
van der Waals JD (1894) Z Phys Chem 13:657
van Saarloos W, Hohenberg PC (1992) Physica D 56:303
van Saarloos W (2003) Phys Rep 386:29
Yang L, Dolnik M, Zhabotinsky AM, Epstein IR (2002) Phys Rev Lett 88:208303
Yochelis A, Elphick C, Hagberg A, Meron E (2004) Physica D 199:201
Zeldovich YB (1985) The mathematical theory of combustion and explosions. Consultants Bureau, New York

Books and Reviews

Cross MC, Hohenberg P (1993) Rev Mod Phys 65:851
Epstein IR, Pojman JA (1998) Introduction to nonlinear chemical dynamics. Oxford University Press, New York
Fife PC (1979) Mathematical aspects of reacting and diffusing systems. Springer, Berlin
Haken H (2004) Synergetics: introduction and advanced topics. Springer, Berlin
Hoyle R (2006) Pattern formation. Cambridge UP, Cambridge
Kuramoto Y (1984) Chemical oscillations, waves and turbulence. Springer, Berlin

Manneville P (1990) Dissipative structures and weak turbulence. Academic, San Diego
Mikhailov AS (1991) Foundations of synergetics i: distributed active systems II (with AY Loskutov): complex patterns. Springer, Berlin
Murray JD (1989) Mathematical biology. Springer, Berlin; 2nd edn 1993; 3rd edn 2002/2003
Pismen LM (1999) Vortices in nonlinear fields. Clarendon Press, Oxford
Pismen LM (2006) Patterns and interfaces in dissipative dynamics. Springer, Berlin
Rabinovich MI, Ezersky AB, Weidman PD (2000) The dynamics of patterns. World Scientific, Singapore
Walgraef D (1997) Spatio-temporal pattern formation. Springer, New York
Winfree AT (1987) When time breaks down. Princeton University Press, Princeton